

The distribution and physical properties of high-redshift [OIII] emitters in a cosmological hydrodynamics simulation

Kana Moriwaki^{1*}, Naoki Yoshida^{1,2,3}, Ikkoh Shimizu⁴, Yuichi Harikane^{1,5},
 Yuichi Matsuda^{6,7}, Hiroshi Matsuo^{6,7}, Takuya Hashimoto^{6,8}, Akio K. Inoue⁸,
 Yoichi Tamura⁹, Tohru Nagao¹⁰.

¹*Department of Physics, The University of Tokyo, 7-3-1 Hongo, Bunkyo, Tokyo 113-0033, Japan*

²*Kavli Institute for the Physics and Mathematics of the Universe (WPI), UT Institutes for Advanced Study, The University of Tokyo, 5-1-5 Kashiwanoha, Kashiwa, Chiba 277-8583, Japan*

³*Research Center for the Early Universe, School of Science, The University of Tokyo, 7-3-1 Hongo, Bunkyo, Tokyo 113-0033, Japan*

⁴*Theoretical Astrophysics, Department of Earth and Space Science, Osaka University, 1-1 Machikaneyama, Toyonaka, Osaka 560-0043, Japan*

⁵*Institute for Cosmic Ray Research, The University of Tokyo, 5-1-5 Kashiwanoha, Kashiwa, Chiba 277-8582, Japan*

⁶*National Astronomical Observatory of Japan, 2-21-1 Osawa, Mitaka, Tokyo 181-8588, Japan*

⁷*Department of Astronomical Science, School of Physical Sciences, The Graduate University for Advanced Studies (SOKENDAI), 2-21-1 Osawa, Mitaka, Tokyo 181-8588, Japan*

⁸*Department of Environmental Science and Technology, Faculty of Design Technology, Osaka Sangyo University, 3-1-1, Nagaito, Daito, Osaka 574-8530, Japan*

⁹*Division of Particle and Astrophysical Science, Graduate School of Science, Nagoya University, Furo-cho, Chikusa-ku, Nagoya 464-8602, Japan*

¹⁰*Research Center for Space and Cosmic Evolution, Ehime University, 2-5 Bunkyo-cho, Matsuyama, Ehime 790-8577, Japan*

ABSTRACT

Recent observations with the Atacama Large Millimeter/submillimeter Array (ALMA) detected far-infrared emission lines such as the [OIII] 88 μ m line from galaxies at $z \sim 7 - 9$. We use a cosmological simulation of galaxy formation to study the physical properties of [OIII] 88 μ m emitters. In a comoving volume of $50h^{-1}$ Mpc on a side, we locate 34 galaxies with stellar masses greater than $10^8 M_{\odot}$ at $z = 9$, and more than 270 such galaxies at $z = 7$. We calculate the [OIII] 88 μ m luminosities ($L_{\text{OIII},88}$) by combining a physical model of HII regions with emission line calculations using the photoionization code CLOUDY. We show that the resulting $L_{\text{OIII},88}$, for a given star formation rate, is slightly higher than predicted from the empirical relation for local galaxies, and is consistent with recent observations of galaxies at redshifts 7 - 9. Bright [OIII] emitters with $L_{\text{OIII},88} > 10^8 L_{\odot}$ have star formation rates higher than $3 M_{\odot} \text{ yr}^{-1}$, and the typical metallicity is $\sim 0.1 Z_{\odot}$. The galaxies are hosted by dark matter halos with masses greater than $10^{11} M_{\odot}$. We propose to use the [OIII] 5007 \AA line, to be detected by James Webb Space Telescope (JWST), to study the properties of galaxies whose [OIII] 88 μ m line emission have been already detected with ALMA.

Key words: galaxies: evolution — galaxies: high-redshift — galaxies: ISM

1 INTRODUCTION

One of the major goals of the next generation space-borne and ground-based telescopes is to detect and characterize the first galaxies that were in place a few hundred million years after the Big Bang. There has been impressive progress in exploration of the redshift frontier of distant galaxies. Hubble Space Telescope has detected a number of distant galaxies by dropout techniques (Yan et al. 2011;

Ellis et al. 2013; McLure et al. 2013; Schenker et al. 2013; Dunlop et al. 2013; Robertson et al. 2013; Ono et al. 2013; Koekemoer et al. 2013; Oesch et al. 2013; Bouwens et al. 2014; Finkelstein et al. 2015; Bouwens et al. 2015). Intrinsically faint galaxies have also been detected with the help of gravitational lensing magnification (Zheng et al. 2012; Oesch et al. 2015; Ishigaki et al. 2015). Hydrogen Ly α line has been used primarily to determine the spectroscopic redshifts of these galaxies. Unfortunately, the Ly α line becomes increasingly weak at $z > 7$ through the epoch of reioniza-

* E-mail: kana.moriwaki@utap.phys.s.u-tokyo.ac.jp

tion when the intergalactic medium (IGM) neutral fraction increases (e.g. Konno et al. 2014).

Rest-frame far-infrared lines are a promising probe of distant galaxies. The Atacama Large Millimeter/submillimeter Array (ALMA) is capable of detecting multiple far-infrared lines even from galaxies at $z > 7$. Although initial attempts to detect the [CII] 158 μm line, one of the brightest emission lines from star-forming galaxies, resulted in both success and non-detections (Walter et al. 2012; Kanekar et al. 2013; Ouchi et al. 2013), recent observations show that the [CII] 158 μm line can be used to identify and to study the structure and kinematics of distant galaxies (Smit et al. 2018).

[OIII] 88 μm emission is another excellent probe of high-redshift star-forming galaxies. From a theoretical point of view, the [OIII] 88 μm emission is easy to model because it originates from HII regions, unlike the [CII] 158 μm emission which likely originates from both ionized and neutral regions (Nagamine, Wolfe & Hernquist 2006; Pallottini et al. 2017; Lagache, Cousin & Chatzikos 2018). Interestingly, many nearby dwarf galaxies show stronger [OIII] 88 μm emission than [CII] 158 μm (Madden et al. 2012; Lebouteiller et al. 2012; Cormier et al. 2015). Motivated by these observations, Inoue et al. (2014) proposed to use the [OIII] 88 μm line to determine the spectroscopic redshifts of galaxies at $z > 8$. Recent observations using ALMA successfully discovered the [OIII] line from galaxies beyond redshift 7 (Inoue et al. 2016; Carniani et al. 2017; Laporte et al. 2017) and even at $z = 9.11$ (Hashimoto et al. 2018b). In combination with optical/infrared observations and detection of the hydrogen Lyman- α line, the ALMA observations provide rich information on the physical properties of the early galaxies that are thought to have driven cosmic reionization.

With the launch of James Webb Space Telescope (JWST) scheduled in 2021, it is timely and important to study the formation and evolution of early emission line galaxies. To this end, we use a high-resolution cosmological simulation of galaxy formation and study the statistics and physical properties of a population of [OIII] emitters at $z > 7$. Throughout the present Letter, we adopt a ΛCDM cosmology with the matter density $\Omega_{\text{M}} = 0.3175$, the cosmological constant $\Omega_{\Lambda} = 0.6825$, the Hubble constant $h = 0.6711$ in units of $H_0 = 100 \text{ km s}^{-1} \text{ Mpc}^{-1}$ and the baryon density $\Omega_{\text{B}} = 0.04899$. The matter density fluctuations are normalized by setting $\sigma_8 = 0.8344$ (Planck Collaboration et al. 2014).

2 METHODS

We use outputs of a cosmological hydrodynamics simulation of Shimizu et al. (2016). The simulation follows the formation of galaxies in a fully cosmological context by implementing star formation, the stellar feedback effects by radiation pressure and supernova explosions, and multi-element chemical enrichment (Okamoto, Nemmen & Bower 2008; Okamoto et al. 2010; Okamoto, Shimizu & Yoshida 2014; Okamoto & Frenk 2009). The feedback model parameters are chosen to reproduce the observed star-formation rate density from $z = 10$ to $z = 0$, and the galaxy stellar mass functions, the stellar mass - halo mass relation, and the relation between stellar mass and metallic-

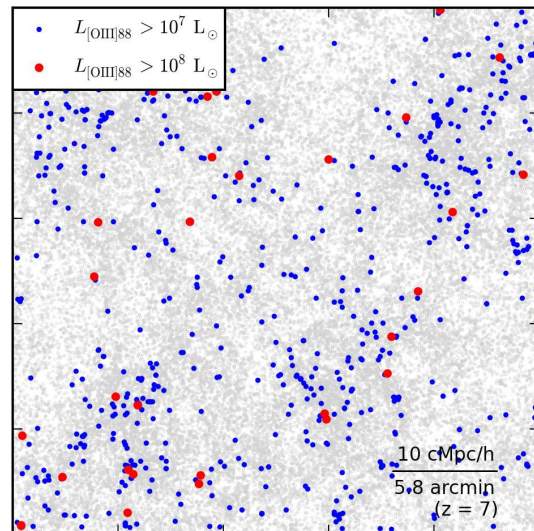


Figure 1. We plot the projected distribution of [OIII] emitters at $z = 7$ in a cubic volume of comoving $50h^{-1} \text{ Mpc}$ ($= 29'$) on a side. The gray points are all the galaxies in this volume, whereas the blue and red points represent galaxies with $L_{\text{OIII},88} > 10^7 L_{\odot}$ and $> 10^8 L_{\odot}$, respectively. The [OIII] 5007 \AA line luminosities can be approximately estimated by multiplying $L_{\text{OIII},88}$ by a factor of ten.

Table 1. The parameters used to calculate the line luminosities with CLOUDY. The metallicities are normalized by $Z_{\odot} = 0.02$.

$\log_{10}(Z/Z_{\odot})$	-2.2, -1.6, -0.6, -0.3, 0.1, 0.5
$\log_{10} U$	-4.0, -3.9, ..., -1.1, -1.0
$\log_{10}(n_{\text{HII}}/\text{cm}^{-3})$	1.0, 2.0, 3.0

ity at $z = 4$ through to $z = 0$. Our simulation reproduces a broad range of the observed features of high-redshift galaxy populations such as Lyman break galaxies, Lyman- α emitters, and sub-mm galaxies as well as those of local galaxies (Shimizu, Yoshida & Okamoto 2012; Shimizu et al. 2014, 2016; Okamoto, Shimizu & Yoshida 2014). The initial conditions are configured with 2×1280^3 gas and dark matter particles in a cubic volume of comoving $50h^{-1} \text{ Mpc}$. The mass of a dark matter particle is $4.44 \times 10^6 h^{-1} M_{\odot}$ and the initial mass of a gas particle is $8.11 \times 10^5 h^{-1} M_{\odot}$. The softening length for the gravitational force is set to be $2h^{-1} \text{ kpc}$ in comoving unit. The details of the simulation are found in Shimizu et al. (2016).

Following the standard star-formation prescription, star particles are spawned in cold and dense gas clouds. The mass of a star particle is as small as $\sim 10^6 M_{\odot}$, and thus galaxies with mass $\sim 10^9 M_{\odot}$ are represented by more than ~ 1000 star particles and gas particles. We study the internal structure of the galaxies on sub-kpc scales such as the relative distributions of young and old stars, and also the distribution of rest-frame optical/far-infrared line emitting regions.

3 SPECTRAL ENERGY DISTRIBUTION OF GALAXIES

We calculate the spectral energy distribution (SED) of each spawned star particle using the population synthesis code PÉGASE2 (Fioc & Rocca-Volmerange 1997). We obtain the total SED of a simulated galaxy by summing the contributions from all the star particles within the galaxy. We adopt the Calzetti law of dust extinction (Calzetti et al. 2000). We calculate the escape probability f_{UV} of ultra-violet (UV) photons at 1500 Å adopting a dust distribution model of Xu & Buat (1995) and Shimizu et al. (2014):

$$f_{UV} = \frac{1 - \delta}{2}(1 + e^{-\tau_d}) + \frac{\delta}{\tau_d}(1 - e^{-\tau_d}), \quad (1)$$

where δ is a parameter whose value is from 0 to 1 and τ_d is the UV optical depth. The optical depth τ_d is calculated in the same way as in Shimizu et al. (2016). With $\delta = 0.95$ for attenuation of continuum, the rest-frame UV luminosity function matches well to the observed ones at $z = 6 - 10$.

The nebular emission line luminosities are calculated in the following manner. We generate a library of emission lines using CLOUDY¹ (Ferland et al. 2013) as in Inoue (2011) and Inoue et al. (2014). The library covers a wide range of gas metallicity Z , ionization parameter U and gas density n_{HII} as given in Table 1. We use the local oxygen abundance y_{O} to derive the corresponding metallicity as $Z = Z_{\odot} \times y_{\text{O}}/y_{\text{O},\odot}$, where $y_{\text{O},\odot}$ is the solar abundance of oxygen.

For the current and future use, the library lists the line luminosity, L_{line} , such that it is normalized by the $\text{H}\beta$ luminosity with the case-B approximation (Dopita & Sutherland 2003), $L_{\text{H}\beta}^{\text{caseB}}$, as

$$L_{\text{line}} = (1 - f_{\text{esc}})C_{\text{line}}(Z, U, n_{\text{HII}})L_{\text{H}\beta}^{\text{caseB}}, \quad (2)$$

where f_{esc} is the Lyman continuum escape fraction and C_{line} is the line luminosity ratio. We assume $f_{\text{esc}} = 0.1$ in the present Letter. The choice of a constant escape fraction may be unrealistic, since it is intrinsically a time-dependent quantity and depends also on a variety of properties such as halo mass and gas clumping. Recent high-resolution radiation hydrodynamics simulations suggest time-averaged escape fractions of several to ten percent for high-redshift galaxies (Trebitsch et al. 2017), which motivate our choice here. Since the line luminosities are proportional to $(1 - f_{\text{esc}})$, other cases with higher/lower f_{esc} can be inferred by scaling the line luminosities correspondingly.

Individual HII regions are not resolved in our simulation, and thus we resort to a simple physical model of the inter-stellar medium (ISM) structure to calculate the emissivities of the lines originating from HII regions. We characterize the ISM by the local gas density n and metallicity Z , and also by a volume-averaged ionization parameter

$$U = \frac{3\alpha_{\text{B}}^{2/3}}{4c} \left(\frac{3Qn_{\text{HII}}}{4\pi} \right)^{1/3}, \quad (3)$$

¹ We configure plane-parallel geometry, and stop the calculations when the fraction of the electron number density and the hydrogen number density becomes lower than 10^{-3} . To generate the source SEDs, we adopt constant star formation with Salpeter initial mass function and use BC03 (Bruzual & Charlot 2003). Note that the difference between BC03 and PÉGASE2 is very small.

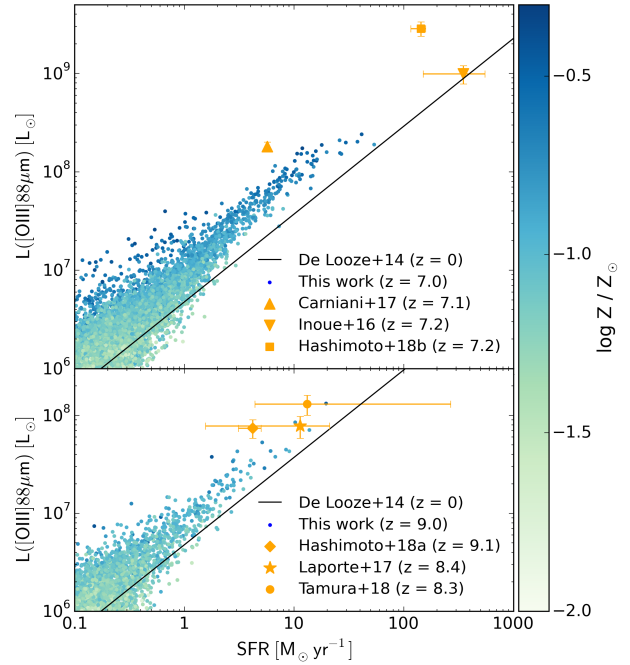


Figure 2. The [OIII] line luminosity against star formation rate of our galaxy samples at $z = 7$ and $z = 9$. We indicate the gas metallicity by the color of each point. We compare them with the observed galaxies at $z = 7 - 9$ (Inoue et al. 2016; Carniani et al. 2017; Laporte et al. 2017; Hashimoto et al. 2018b,a; Tamura et al. 2018). The black line shows the [OIII]-SFR relation derived by De Looze et al. (2014) for all kinds of local galaxies. Note that the galaxy B14-65666 of Hashimoto et al. (2018a) at $z = 7.15$ appears to consist of two clumps.

where Q is the production rate of ionizing photons from each star particle, and α_{B} is the case-B hydrogen recombination coefficient. Essentially, we assume a constant gas density n_{HII} in a spherical HII region surrounding a star particle (e.g. Panuzzo et al. 2003; Hirschmann et al. 2017). We assume that the HII region density is given by $n_{\text{HII}} = Kn$, where n is the gas particle density in the vicinity of the star particle, so that compact galaxies tend to have large n_{HII} . With $K = 5$ as our fiducial value, n_{HII} ranges approximately from 30 to 300 cm^{-3} , which is the typical range of the HII region density (e.g. Osterbrock & Ferland 2006; Brinchmann, Pettini & Charlot 2008). We note that different methods, as well as different numerical resolutions, may slightly change the estimated [OIII] luminosities.

4 RESULTS

Figure 1 shows the spatial distribution of the [OIII] emitters identified at $z = 7$. The blue and red points represent galaxies with $L_{\text{OIII},88} > 10^7 L_{\odot}$ and $> 10^8 L_{\odot}$, respectively. The [OIII] emitters are strongly clustered, and trace the large-scale structure of ~ 10 Mpc scales. We calculate the two-point correlation function of the bright [OIII] emitters. The clustering bias of galaxies with $L_{\text{OIII},88} > 10^7 L_{\odot}$ is 4.0 at a separation of $3h^{-1}$ comoving mega-parsec.

The early large-scale structure and its evolution can be probed by future observations with JWST NIRCcam target-

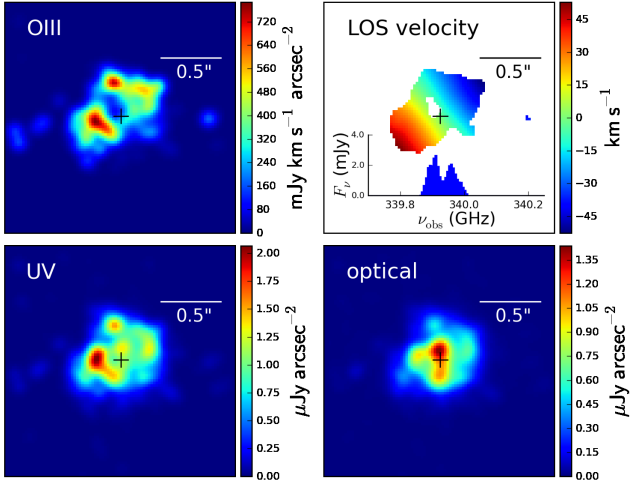


Figure 3. The structure of a galaxy at $z = 9$ with $M_* = 6.3 \times 10^8 M_\odot$, $M_{\text{halo}} = 8.2 \times 10^{10} M_\odot$, $\text{SFR} = 4.9 M_\odot/\text{yr}$, and $L_{\text{OIII},88} = 5.4 \times 10^7 L_\odot$. We plot the [OIII] $88\mu\text{m}$ flux, the [OIII] luminosity weighted line-of-sight gas velocity, the rest-frame UV continuum (1600 \AA) flux and the rest-frame optical continuum (5000 \AA) flux. The cross indicates the mass center of the stars. For this figure, we assume that the galaxy is gravitationally lensed with $\mu = 10$, to be compared with, e.g., MACS1149-JD1 (Hashimoto et al. 2018b). The inset of the upper right panel shows the spectrum to be observed with ALMA.

ing rest-frame optical emission lines such as [OIII] 5007\AA , as we propose in the Discussion section, or by utilizing the intensity mapping technique at sub-millimeter wavelengths (Visbal & Loeb 2010). Our simulation predicts that the total [OIII] $88\mu\text{m}$ luminosity at $z = 7$ in a cubic volume of comoving $50h^{-1} \text{ Mpc}$ is $2.2 \times 10^{10} L_\odot$, giving a significant contribution to the global sub-millimeter line intensity.

In Figure 2, we plot $L_{\text{OIII},88}$ against star-formation rate (SFR) for our emission line galaxy samples. For reference, we also show the $L_{\text{OIII},88}$ -SFR relation for all kinds of local galaxies derived by De Looze et al. (2014). Our model predicts slightly larger values of $L_{\text{OIII},88}$ than the local relation; early galaxies tend to be compact and have large ionization parameters. Several galaxies in the simulated volume have $L_{\text{OIII},88}$ and SFRs comparable to the intrinsic $L_{\text{OIII},88}$ and SFRs of the galaxies recently identified at $z \sim 7 - 9$ (Carniani et al. 2017; Laporte et al. 2017; Hashimoto et al. 2018b). The bright [OIII] emitters have metallicities of $\sim 0.1 Z_\odot$, consistent with the estimate of, e.g., Inoue et al. (2016). The [OIII] emitters with $L_{\text{OIII},88} > 10^8 L_\odot$ at $z = 7$ are hosted by dark matter halos with mass greater than $10^{11} M_\odot$.

Some bright [OIII] emitters have extended structure of ~ 1 physical kilo-persec. We find that the [OIII] $88\mu\text{m}$ emitting regions are localized and sometimes displaced from the bulk stellar distribution. This is because the stellar distribution traces the regions where prior star-formation activities have already consumed the gas, while on-going star-formation in other places powers the instantaneous [OIII] emission. Figure 3 shows the structure of one of the brightest galaxies at $z = 9$. Motivated by the intriguing observation of a gravitationally lensed galaxy MACS1149-JD1 (Hashimoto et al. 2018b), we generate Figure 3 assuming

an isotropic lensing magnification of $\mu = 10$. With the help of lensing, the effective physical resolution increases by a factor of ~ 3 .

Both of the [OIII] $88\mu\text{m}$ line emission and the UV continuum trace young stellar populations with ages shorter than several million years. Though the relative displacement between the two distributions is often found for our bright galaxy samples, the flux peaks roughly coincide with each other, consistent with the observed galaxies at $z \sim 7 - 9$ (Inoue et al. 2016; Hashimoto et al. 2018b). We note that there can also be spatial offsets between the [OIII] $88\mu\text{m}$ and the UV emission caused by an inhomogeneous dust distribution (Katz et al. 2017).

5 DISCUSSION

Conventional optical line diagnostics can be used to study the physical properties of the early star-forming galaxies. We calculate the [OIII] 5007\AA luminosity function and compare it with the luminosity function of [OIII] $88\mu\text{m}$ (Figure 4). The vertical lines in the figure indicate typical detection limits of ALMA and JWST. As expected, the [OIII] 5007\AA luminosity is roughly an order of magnitude larger than that of [OIII] $88\mu\text{m}$. Clearly, JWST can detect [OIII] 5007\AA line emission from the galaxies whose [OIII] $88\mu\text{m}$ lines (will) have been detected with ALMA.

The superb spectral and angular resolution of JWST NIRSpec IFU spectroscopy will enable us to study the structure and the kinematics of galaxies at $z > 7$. Gravitational lensing greatly helps not only by increasing the apparent flux of distant galaxies, but also by increasing the effective ‘physical’ spatial resolution. The sub-arcsecond resolutions of ALMA and JWST can be fully exploited to study the fine structure of lensed galaxies even at sub-kiloparsec scales. Signatures of the galaxy’s rotation can be also seen as the line-of-sight velocity gradient of $\Delta v \sim 100 \text{ km s}^{-1}$ (see the upper-right panel of Figure 3).

Future observations with ALMA and JWST hold promise to understand the formation and evolution of the first galaxies. Combining with fully resolved observations of other rest-frame optical and far-infrared emission lines originating from hydrogen, carbon and oxygen in a variety of phases in the ISM, and also with dust continuum emission, we will be able to study the chemical evolution and the ISM structure and kinematics of the galaxies a few to several hundred million years after the Big Bang. It is important to explore theoretically pan-chromatic approaches to elucidate the nature of the first galaxies.

The large-scale distribution of the [OIII] emitters can be probed by using JWST NIRCcam, either by using its narrow band filters or with its grism spectroscopy mode. For instance, the line sensitivity for the NIRCcam grism module at the F444W band is $\sim 3.4 \times 10^{-18} \text{ erg s}^{-1} \text{ cm}^{-2}$ for $\text{S/N} = 5$ with a 10^4 second exposure. It is expected from Figure 1 and 4 that, within the field-of-view of $2 \times 2.2' \times 2.2'$, there will be several [OIII] 5007\AA emitters on average detected in the redshift range of $6.8 < z < 9.0$. Multiple pointings or mosaic observations will map the three-dimensional distribution of [OIII] emitters in the redshift range.

Systematic surveys with JWST NIRCcam narrow-bands can also probe the large-scale structure at $z > 8$. If we per-

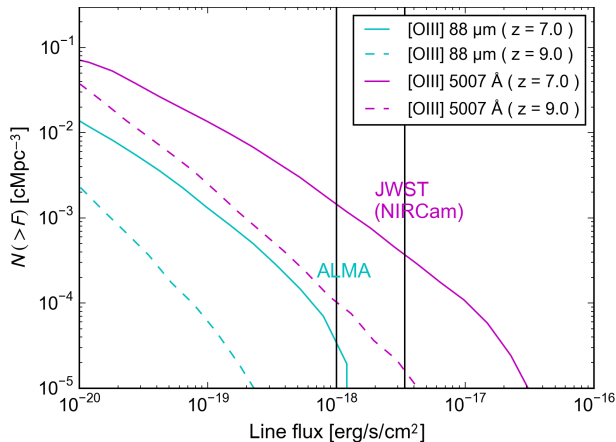


Figure 4. The cumulative line luminosity function for [OIII] 88 μ m (cyan lines) and [OIII] 5007 Å (magenta lines). The solid lines and the dotted lines show the data of $z = 7$ and $z = 9$ respectively. Vertical lines represent typical detection limits of ALMA and JWST NIRCам grism mode assuming 10^4 second integration and the signal-to-noise ratio of 5.

form a narrow-band survey using the F466N filter with the same exposure, we can detect, with $S/N = 5$, $z = 8.3$ [OIII] emitters with line fluxes above $\sim 6.6 \times 10^{-19}$ erg s $^{-1}$ cm $^{-2}$. This limit roughly corresponds to detecting the galaxies shown by blue points in Figure 1. In such narrow-band surveys, foreground H α emitters are severe contaminants, or can actually be major targets at the corresponding wavelength (Silva et al. 2018), but one can use J -dropout technique to select [OIII] 5007Å emitters. We have found that the [OIII] emitters at $z = 8.3$ in our simulation are separated typically by $Y_{105} - J_{125} > 1.0 - 1.5$ from H α emitters at $z = 6.2$. It is possible to select preferentially the [OIII] emitters if we choose and survey a region where deep broad-band data are available.

Future space missions such as Spectrophotometer for the History of the Universe, Epoch of Reionization, and Ice Explorer (SPHEREx) and Cosmic Dawn Intensity Mapper (CDIM) utilize the infrared intensity mapping technique to probe the large-scale galaxy distribution at high-redshifts (Cooray et al. 2016; Doré et al. 2016). Redshifted [OIII] 5007Å emission from early star-forming galaxies such as those studied in the present Letter is an excellent target, and thus serve as a valuable cosmological probe.

ACKNOWLEDGMENTS

The authors thank the anonymous referee for providing us with many insightful comments. This research was supported by the Munich Institute for Astro- and Particle Physics (MIAPP) of the DFG cluster of excellence "Origin and Structure of the Universe". K.M. has been supported by Advanced Leading Graduate Course for Photon Science (ALPS) of the University of Tokyo. I.S., Y.H., Y.M., A.K.I. and Y.T. acknowledge JSPS KAKENHI grants 26247022, 17H01111 (I.S.), 16J03329 (Y.H.), 17H04831, 17KK0098 (Y.M.), 17H01114 (A.K.I) and 17H06130 (Y.T.). T.H., A.K.I. and Y.T. acknowledge the NAOJ ALMA Scientific Re-

search Grand number 2016-01A (T.H., A.K.I) and 2018-09B (Y.T.).

REFERENCES

- Bouwens R. J. et al., 2014, ApJ, 793, 115
 Bouwens R. J. et al., 2015, ApJ, 803, 34
 Brinchmann J., Pettini M., Charlot S., 2008, MNRAS, 385, 769
 Bruzual G., Charlot S., 2003, MNRAS, 344, 1000
 Calzetti D., Armus L., Bohlin R. C., Kinney A. L., Koornneef J., Storchi-Bergmann T., 2000, ApJ, 533, 682
 Carniani S. et al., 2017, A&A, 605, A42
 Cooray A. et al., 2016, ArXiv e-prints
 Cormier D. et al., 2015, A&A, 578, A53
 De Looze I. et al., 2014, A&A, 568, A62
 Doré O. et al., 2016, ArXiv e-prints
 Dunlop J. S. et al., 2013, MNRAS, 432, 3520
 Ellis R. S. et al., 2013, ApJ, 763, L7
 Ferland G. J. et al., 2013, Rev. Mexicana Astron. Astrofis., 49, 137
 Finkelstein S. L. et al., 2015, ApJ, 810, 71
 Fioc M., Rocca-Volmerange B., 1997, A&A, 326, 950
 Hashimoto T. et al., 2018a, ArXiv e-prints
 Hashimoto T. et al., 2018b, Nature, 557, 392
 Hirschmann M., Charlot S., Feltre A., Naab T., Choi E., Ostriker J. P., Somerville R. S., 2017, MNRAS, 472, 2468
 Inoue A. K., 2011, MNRAS, 415, 2920
 Inoue A. K., Shimizu I., Tamura Y., Matsuo H., Okamoto T., Yoshida N., 2014, ApJ, 780, L18
 Inoue A. K. et al., 2016, Science, 352, 1559
 Ishigaki M., Kawamata R., Ouchi M., Oguri M., Shimasaku K., Ono Y., 2015, ApJ, 799, 12
 Kanekar N., Wagg J., Chary R. R., Carilli C. L., 2013, ApJ, 771, L20
 Katz H., Kimm T., Sijacki D., Haehnelt M. G., 2017, MNRAS, 468, 4831
 Koekemoer A. M. et al., 2013, ApJS, 209, 3
 Konno A. et al., 2014, ApJ, 797, 16
 Lagache G., Cousin M., Chatzikos M., 2018, A&A, 609, A130
 Laporte N. et al., 2017, ApJ, 837, L21
 Leboutteiller V. et al., 2012, A&A, 548, A91
 Madden S. C., Rémy A., Galliano F., Galametz M., Bendo G., Cormier D., Leboutteiller V., Hony S., 2012, in IAU Symposium, Vol. 284, The Spectral Energy Distribution of Galaxies - SED 2011, Tuffs R. J., Popescu C. C., eds., pp. 141–148
 McLure R. J. et al., 2013, MNRAS, 432, 2696
 Nagamine K., Wolfe A. M., Hernquist L., 2006, ApJ, 647, 60
 Oesch P. A., Bouwens R. J., Illingworth G. D., Franx M., Ammons S. M., van Dokkum P. G., Trenti M., Labbé I., 2015, ApJ, 808, 104
 Oesch P. A. et al., 2013, ApJ, 773, 75
 Okamoto T., Frenk C. S., 2009, MNRAS, 399, L174
 Okamoto T., Frenk C. S., Jenkins A., Theuns T., 2010, MNRAS, 406, 208
 Okamoto T., Nemmen R. S., Bower R. G., 2008, MNRAS, 385, 161
 Okamoto T., Shimizu I., Yoshida N., 2014, PASJ, 66, 70

- Ono Y. et al., 2013, *ApJ*, 777, 155
Osterbrock D. E., Ferland G. J., 2006, *Astrophysics of gaseous nebulae and active galactic nuclei*.
Ouchi M. et al., 2013, *ApJ*, 778, 102
Pallottini A., Ferrara A., Gallerani S., Vallini L., Maiolino R., Salvadori S., 2017, *MNRAS*, 465, 2540
Panuzzo P., Bressan A., Granato G. L., Silva L., Danese L., 2003, *A&A*, 409, 99
Planck Collaboration et al., 2014, *A&A*, 571, A16
Robertson B. E. et al., 2013, *ApJ*, 768, 71
Schenker M. A. et al., 2013, *ApJ*, 768, 196
Shimizu I., Inoue A. K., Okamoto T., Yoshida N., 2014, *MNRAS*, 440, 731
Shimizu I., Inoue A. K., Okamoto T., Yoshida N., 2016, *MNRAS*, 461, 3563
Shimizu I., Yoshida N., Okamoto T., 2012, *MNRAS*, 427, 2866
Silva B. M., Zaroubi S., Kooistra R., Cooray A., 2018, *MNRAS*, 475, 1587
Smit R. et al., 2018, *Nature*, 553, 178
Tamura Y. et al., 2018, *ArXiv e-prints*
Trebitsch M., Blaizot J., Rosdahl J., Devriendt J., Slyz A., 2017, *MNRAS*, 470, 224
Visbal E., Loeb A., 2010, *J. Cosmology Astropart. Phys.*, 11, 016
Walter F. et al., 2012, *ApJ*, 752, 93
Xu C., Buat V., 1995, *A&A*, 293
Yan H. et al., 2011, *ApJ*, 728, L22
Zheng W. et al., 2012, *Nature*, 489, 406